PHYSICS

Angle-multiplexed all-dielectric metasurfaces for broadband molecular fingerprint retrieval

Aleksandrs Leitis[1]*, Andreas Tittl[1]*, Mingkai Liu[2], Bang Hyun Lee[3], Man Bock Gu[3], Yuri S. Kivshar[2], Hatice Altug[1†]

Infrared spectroscopy resolves the structure of molecules by detecting their characteristic vibrational fingerprints. Subwavelength light confinement and nanophotonic enhancement have extended the scope of this technique for monolayer studies. However, current approaches still require complex spectroscopic equipment or tunable light sources. Here, we introduce a novel metasurface-based method for detecting molecular absorption fingerprints over a broad spectrum, which combines the device-level simplicity of state-of-the-art angle-scanning refractometric sensors with the chemical specificity of infrared spectroscopy. Specifically, we develop germanium-based high-*Q* metasurfaces capable of delivering a multitude of spectrally selective and surface-sensitive resonances between 1100 and 1800 cm^{-1}. We use this approach to detect distinct absorption signatures of different interacting analytes including proteins, aptamers, and polylysine. In combination with broadband incoherent illumination and detection, our method correlates the total reflectance signal at each incidence angle with the strength of the molecular absorption, enabling spectrometer-less operation in a compact angle-scanning configuration ideally suited for field-deployable applications.

INTRODUCTION

Optical sensors, where the properties of a target sample are inferred from light scattered or absorbed by it, are important for applications in diverse fields including security, environmental monitoring, bioanalytics, and diagnostics (*1*–*4*). Because these sensors operate in the optical far-field regime, they are inherently noninvasive in addition to providing high sensitivities. In biochemical detection, label-free optical techniques are of particular interest since they provide a toolkit for measuring molecular concentrations and interaction kinetics without interference from fluorescent labels or other external tags (*5*, *6*). Surface plasmon resonance (SPR) biosensors are the established gold standard in label-free technology, both in laboratory settings and commercial applications (*7*, *8*). SPR techniques are based on the resonant excitation of electromagnetic surface waves at a metal-dielectric interface, which provides a resonance that is highly sensitive to the refractive index of the surrounding analyte. One of the most common SPR device implementations is angle scanning, where momentum conservation is used to retrieve the resonance line shape using a single-wavelength source and a broadband detector. Overall, this approach provides low device-level complexity and does not require the use of a bulky and expensive spectrometer for accessing the refractometric response of the resonance. Although such refractometric methods can detect the presence of specific molecules in combination with suitable surface functionalization, they lack the capability of ab initio chemical identification. Chemically specific optical detection is enabled by the distinct absorption signatures of chemical and biological analytes at infrared (IR) frequencies (*9*, *10*). In particular, every molecule is characterized by the vibrational modes and associated absorption bands of its chemical bonds, which form the unique absorption fingerprint of the material.

Molecular absorption signatures are commonly accessed using mid-IR spectroscopy techniques, which can be combined with resonant metasurfaces to enhance and retrieve fingerprints from low amounts of molecules and monolayer samples (*11*–*13*). Recently, surface-enhanced IR absorption methods have been emerging as powerful tools for resolving complex molecular interactions in chemical or biological systems with high sensitivity (*11*, *14*). So far, metal-based resonant plasmonic antenna geometries have predominantly been used to provide tailored absorption enhancement but face fundamental limitations due to the intrinsic damping of the metals (*15*). This constraint can be addressed by introducing low-loss dielectric metasurfaces made out of materials such as amorphous silicon (*16*, *17*), gallium arsenide (*18*), or chalcogenide glasses (*19*). By providing high resonance quality (*Q*) factors, all-dielectric metasurfaces can enable highly sensitive surface-enhanced detection of biomolecules, polymers, and environmental toxins with new device implementations (*20*). As a resonator material, germanium offers opportunities for improving the performance of dielectric sensors due to its higher refractive index and lower absorption losses in the mid-IR compared to silicon (*21*).

In this article, we introduce a germanium-based metasurface sensor that combines chemically specific broadband IR detection with the device-level simplicity and spectrometer-less operation of angle-scanning refractometric approaches. Specifically, we implement a nanophotonic resonator design that provides a highly surface-sensitive and spectrally sharp resonance, where the spectral position can be controlled with the incidence angle of the mid-IR light. This angle-multiplexed approach delivers a large number of on-demand resonances in the mid-IR from a single metasurface chip, only limited by the range of light incidence angles. For angular positions in which the resonances match the vibrational modes of analyte molecules, a strong modulation of the far-field optical response occurs because of highly accessible surface-enhanced electric near fields. By retrieving the angle-resolved reflectance signal from such metasurface before and after coating with the analyte molecules, the full spectral content of the molecular absorption fingerprint can be retrieved. We experimentally realize a metasurface capable of providing more than 200 resonances when illuminated with incidence angles ranging from 13° to 60° and use the resulting wide spectral coverage between 1100 and 1800 cm^{-1} with a 1.4 cm^{-1} resonance

[1]Institute of Bioengineering, École Polytechnique Fédérale de Lausanne (EPFL), Lausanne 1015, Switzerland. [2]Nonlinear Physics Centre, Australian National University, Canberra, ACT 2601, Australia. [3]Department of Biotechnology, College of Life Sciences and Biotechnology, Korea University, Seoul, Republic of Korea.
*These authors contributed equally to this work.
†Corresponding author. Email: hatice.altug@epfl.ch

step size to demonstrate chemically specific detection of different molecular analytes such as polymers, proteins, and DNA. Specifically, we implemented a multianalyte bioassay to detect human odontogenic ameloblast-associated protein (ODAM) by using single-stranded DNA aptamers, which has strong implications for diagnosing periodontal diseases. Last, we show that our method is capable of retrieving spectrally resolved molecular fingerprint information even when used with incoherent broadband light sources and detectors, paving the way toward compact and low-cost mid-IR sensors.

RESULTS

Angle-multiplexed metasurface sensor concept

Angle multiplexing is a powerful concept that allows encoding of different values of optical parameters such as polarization or phase on a single metasurface (*22*), unlocking additional degrees of freedom in realizing versatile nanophotonic devices. However, so far, this flexibility has not been leveraged for sensing or spectroscopy applications. Our angle-multiplexed device is designed to resonantly reflect in a narrow spectral range around a frequency ν at each incidence angle θ when illuminated with a broadband source (Fig. 1A). This optical response is provided by a dielectric metasurface consisting of an anisotropic zigzag array of germanium resonators on a calcium fluoride (CaF_2) substrate, which interact collectively to generate ultrasharp resonances in reflection. Crucially, the metasurface provides a monotonic relationship between the resonance frequency and the incidence angle, allowing us to uniquely associate every angular position with a specific target frequency in the spectral working range (Fig. 1A, bottom).

Our high-*Q* metasurface design not only provides angle-multiplexing capabilities but also supports strongly enhanced electric near fields in the vicinity of the resonators, leading to high surface sensitivity. Near-field coupling to adsorbed analyte molecules causes a pronounced attenuation of the resonance line shape dependent on the strength of the absorption bands (Fig. 1B). The high surface sensitivity combined with the spectrally selective resonant reflection for specific incidence angles enables the implementation of a compact sensor device consisting of a broadband source, two mirrors on coaxially rotating arms, and a broadband detector (Fig. 1C).

Our angle-multiplexed fingerprint retrieval (AFR) method detects samples on the sensor surface by measuring the analyte-induced light intensity change at each incidence angle. By combining signal measurements at all angular steps, the absorption spectrum of the analyte is recovered. The output of such an AFR device is uniquely determined by the magnitude and spectral location of the vibrational bands of the analyte, which are correlated with the imaginary part *k* of the complex refractive index $\tilde{n} = n + ik$ (Fig. 1D).

The fundamental building block of our metasurface design is a rectangular unit cell featuring two elliptical germanium resonators on top of a CaF_2 substrate, where the main ellipse axes are tilted asymmetrically with respect to each other to produce a zigzag array (Fig. 2A). The structure height is 800 nm, while the ellipse short and long axis are 900 and 2250 nm, respectively, with an orientation angle of 10° against the *y*

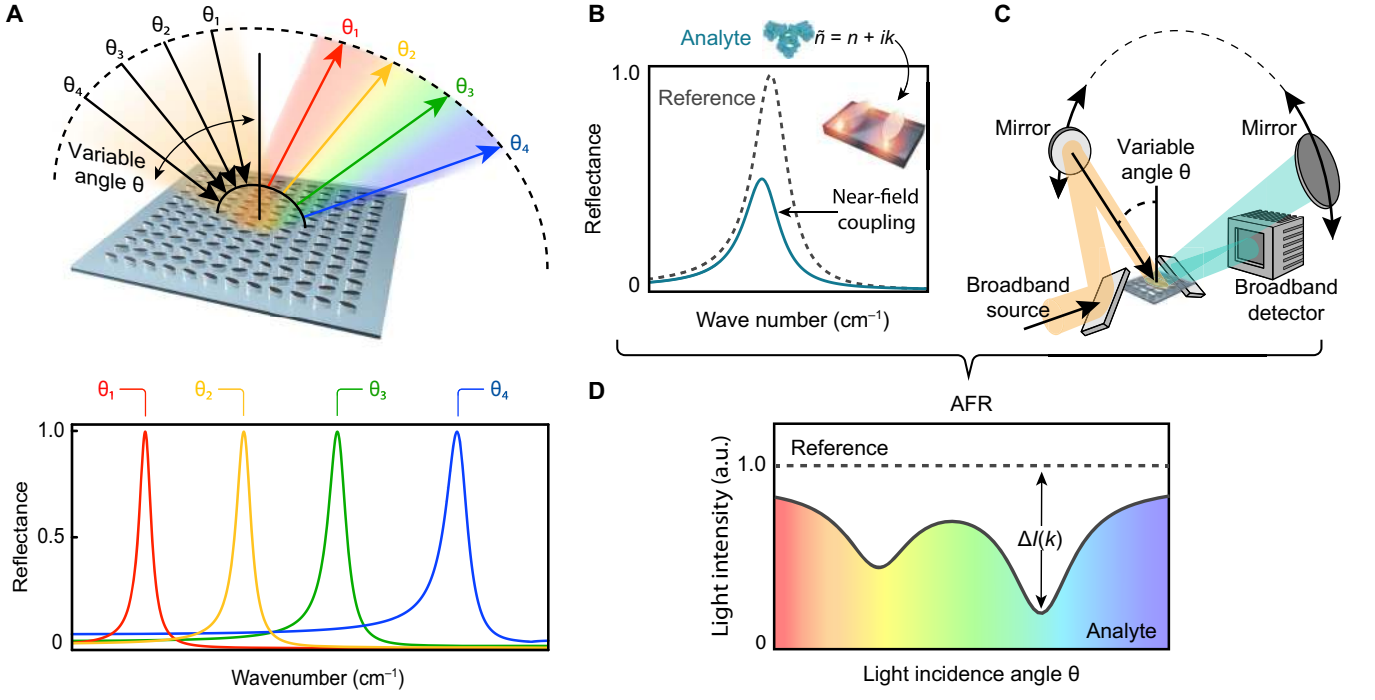

Fig. 1. Angle-multiplexed broadband fingerprint retrieval. (**A**) A germanium-based high-*Q* all-dielectric metasurface delivers ultrasharp on-demand resonances with specific resonance frequency ν for every incidence angle θ with broad spectral coverage. Continuous scanning of the incidence angle produces a multitude of resonances over a target fingerprint range, realizing an angle-multiplexed configuration ideally suited for surface-enhanced mid-IR molecular absorption spectroscopy. (**B**) Strong near-field coupling between the dielectric resonators and the molecular vibrations of the analyte induces a pronounced attenuation of the resonance line shape correlated with the vibrational absorption bands. (**C**) Angle multiplexing combined with the spectral selectivity of high-*Q* resonances allows for broadband operation and straightforward device implementation. (**D**) Chemically specific output signal of the device scheme from (C), which is determined by the imaginary part *k* of the analyte's complex refractive index $\tilde{n}$ (a.u., arbitrary units).

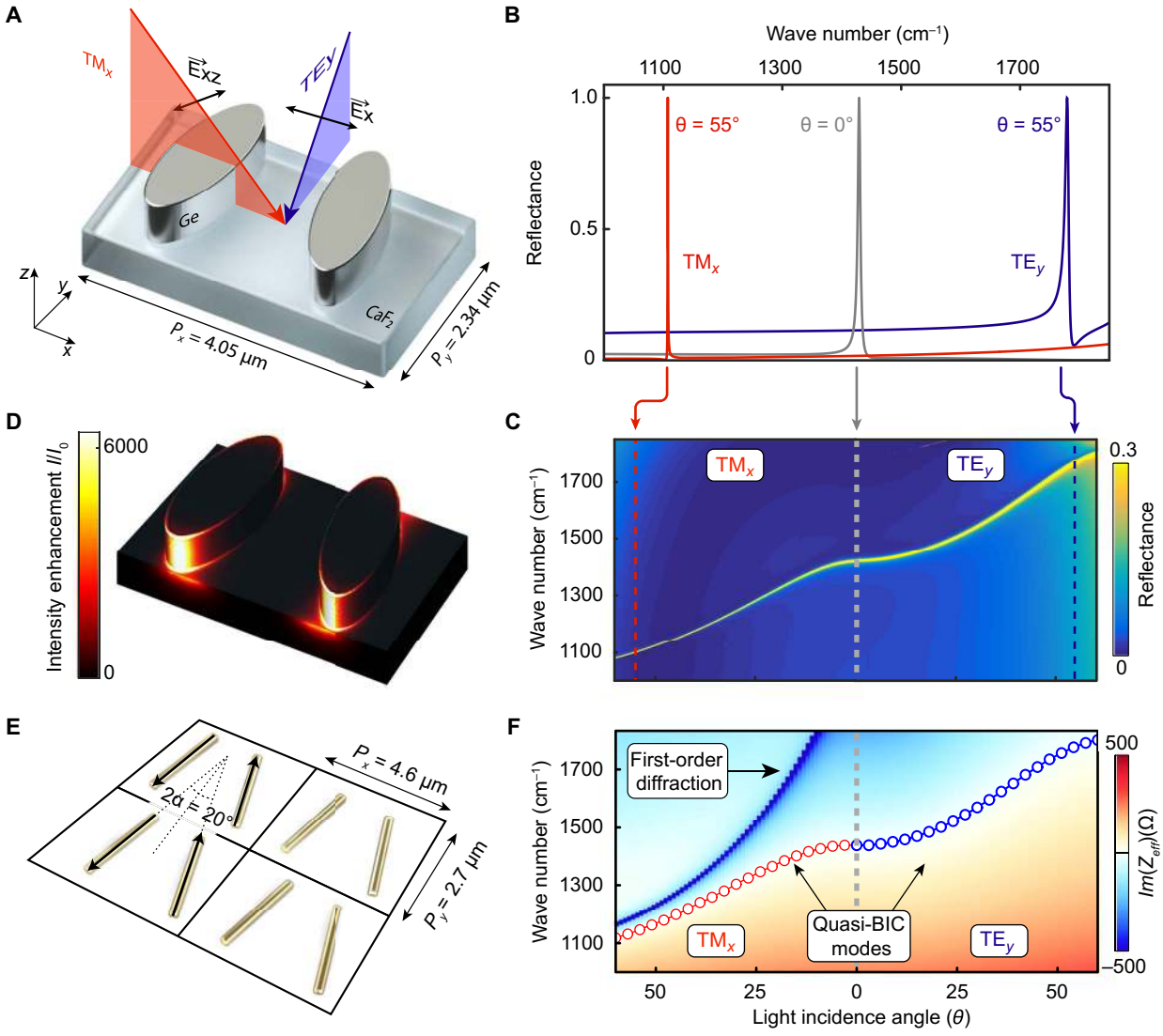

Fig. 2. Working principle of the angle-multiplexed metasurface. (**A**) The dielectric metasurface design consists of a zigzag array of elliptical germanium resonators on a calcium fluoride substrate. When varying the incidence angle, we consider both the TM$_x$ (red plane) and the TE$_y$ (blue plane) modes. (**B**) Simulated reflectance spectra for normal incidence and for an incidence angle of θ = 55° in both TM$_x$ and TE$_y$ modes. The two modes show similar spectral shifts of around 300 cm^{-1}, but in opposite shift directions, enabling wide spectral coverage with a single metasurface design. (**C**) Full resonance dispersion curves (color-coded reflectance) versus incidence angle illustrate the continuous tunability of ultrasharp resonances over the target wave number range together with the spectrally opposite behavior of the TM$_x$ and TE$_y$ modes. (**D**) Because of the highly accessible and strongly enhanced electromagnetic near fields around the resonators, our design is ideally suited for amplifying and detecting the molecular vibrations of adsorbed analytes. (**E**) Zigzag array of line dipoles embedded in a homogeneous environment with a unity refractive index. The length and the orientation angle of the dipoles are 2.7 μm and α = ±10°, respectively. (**F**) Effective reactance $Im(Z_{eff})$ of the quasi-BIC as a function of the incident angle under different excitation modes. The circles mark the positions where the reactance is equal to zero, which determine the angle-dependent resonance frequencies of the quasi-BIC.

axis. When excited with light polarized along the *x* axis at normal incidence, this metasurface based on symmetry-broken elements is capable of delivering an ultrasharp resonance ($Q > 200$) with low spectral background (Fig. 2B), originating from the physics of bound states in the continuum (BIC) (*23*, *24*). These types of interference-governed resonant states were originally introduced in quantum mechanics but have since been extended to other branches of wave physics such as acoustics and optics (*24*–*26*). On a fundamental level, a BIC can be considered as a localized state with vanishing fields within a continuous spectrum of radiating waves. Consequently, an ideal BIC would exhibit an infinite *Q*-factor and would be inaccessible for electromagnetic probes from the far field. To access and exploit these states in metasurface optics, quasi-BIC can be realized by breaking the symmetry of the underlying resonant structure (*23*) as shown in Fig. 2A. In addition, germanium provides negligible intrinsic material losses over the full mid-IR range, further supporting the formation of high-*Q* resonant modes.

The metasurface resonance can be excited as long as the incident light provides a nonzero electric field component along the *x* axis. Therefore, we can scan the light incidence angle in two different planes (*yz* and *xz*) of the unit cell while maintaining efficient metasurface operation. These two ways of exciting the system will be designated as "modes" from now on. Specifically, the first mode (TE$_y$) describes

light with k vector in the yz plane and light polarization along the x axis. The second mode (TM_x) refers to k vector and polarization along the xz plane. Numerical simulations of the metasurface confirm the formation of an ultrasharp resonance line shape in reflection with a Q-factor of 270 at normal light incidence (Fig. 2B). In addition, the numerical data demonstrate a spectrally clean resonance with a low background reflectance. The resonance can be shifted toward either higher or lower wave numbers for increasing incidence angles depending on which mode is used.

To further quantify the resonance tuning behavior, we calculate and plot the full angular dispersion of the metasurface reflectance spectra. The use of both the TE_y and TM_x resonance modes enables an extremely wide and continuous spectral tuning range from 1080 to 1820 cm^{-1} for incidence angles between 0° and 60° (Fig. 2C). The resonance remains spectrally clean with low background reflectance over the full tuning range and provides a monotonous relationship between resonance frequency and light incidence angle. In addition to the angular tunability, the high-Q dielectric metasurface strongly amplifies the electric near fields around the resonators with intensity enhancement factors I/I_0 of up to 6000 (Fig. 2D). Advantageously, the highly enhanced near fields are mostly located on the outer surface of the resonators, making our nanophotonic design very attractive for sensing applications.

The remarkable resonance frequency angular sensitivity can be explained by the collective nature of the quasi-BIC, where the retardation among meta-atoms plays a crucial role in determining the resonant properties of the collective mode. We can develop a deeper understanding of this behavior by modeling the system as an effective medium and considering its impedance $Z_{eff} = -i\omega L_{eff} + i/(\omega C_{eff}) + R_{eff}$, which is calculated from the effective inductance L_{eff}, capacitance C_{eff}, and resistance R_{eff} of the quasi-BIC. These effective parameters can be derived from the lattice sum of the complex electromagnetic interaction of the array with retardation taken into account (*27*). Since the scattered field from an in-plane electric dipole is intrinsically anisotropic in the plane of the metasurface, the electromagnetic interaction of the meta-atoms is also anisotropic. As a result, the lattice sum of the electromagnetic interaction provides different responses when retardation is increased along either the x or y axis of the unit cell under oblique excitation (see the Supplementary Materials). This effect can lead to an opposite resonance shift of the quasi-BIC when the plane of incidence changes from xz (TM_x mode) to yz (TE_y mode). Our analysis reveals that this behavior is a general feature of zigzag dipole arrays made from different materials, which can be observed even in a simple zigzag array of line dipoles embedded in an isotropic medium with a unity refractive index (Fig. 2E). The calculated effective impedance of the line dipoles is shown in (Fig. 2F), where the circles mark the zeros of the imaginary part of the effective impedance $Im(Z_{eff}) = 0$, which determine the angle-dependent resonance frequencies of the quasi-BIC. For further details on the effective impedance and inductance calculations, see the Supplementary Materials (figs. S1 and S2).

Angle-multiplexed fingerprint retrieval

The germanium-based sensor metasurface was fabricated via top-down electron beam lithography on a CaF_2 substrate. For compatibility with open beam angle–scanning measurements, a large-area metasurface with an approximate diameter of 4 mm was realized to fully cover the incident light beam (Fig. 3A). Scanning electron microscopy images show excellent uniformity of the resonator structure sizes over such a large area together with the accurate reproduction of the individual resonator geometry (Fig. 3B). The minimum gap size between adjacent resonators is above 200 nm, which is suitable for high-throughput fabrication methods such as soft-imprint lithography (Fig. 3C).

The metasurface optical performance was characterized with a Fourier transform IR (FTIR) spectrometer (Bruker Vertex 70v) equipped with a variable angle reflection accessory (Bruker A519/Q). We chose an angular range between $\theta = 13°$ and $\theta = 60°$ with 0.2° angular resolution, which resulted in a total of 236 acquired reflectance spectra per angle scan. The minimum scan angle of 13° is due to the mechanical limitations related to the size of the mirrors in the variable angle accessory.

Normalized reflectance spectra for both TE_y and TM_x excitations are shown in (Fig. 3D). For presentation, a subset of all spectra with an average peak position separation of 15 cm^{-1} is chosen to improve clarity. The high-Q resonant behavior with low background reflection is in good agreement with the simulated results. In addition, the experiments confirm the wide resonance frequency tunability from 1120 to 1805 cm^{-1} with an average resonance step size of 1.45 cm^{-1}. The resonance quality factor remains high for all incidence angles with an average Q-factor of 121 (fig. S3), enabling high sensitivity and spectral selectivity throughout a broad spectrum covering a multitude of distinct molecular fingerprints. The resonance step resolution could be improved further by using commercially available rotation stages with angular resolution below 3×10^{-4} degrees, which would increase the number of resonances by more than two orders of magnitude compared to our experiments.

To assess the surface sensitivity of the dielectric metasurface, we spin-coated a thin film of polymethyl methacrylate (PMMA) onto the chip. The normalized reflectance spectra after PMMA deposition show strong attenuation of the reflectance peaks correlated with the vibrational bands of the polymer (Fig. 3E). To further quantify the retrieved absorption signature of the PMMA, we calculated the absorbance $A(\theta)$ from the peak reflectance amplitudes R_0 and R_A at each incidence angle before and after polymer coating following $A(\theta) = -\log_{10}(R_A/R_0)$ (Fig. 3F).

For comparison, a standard IR reflection absorption spectroscopy (IRRAS) measurement was performed with a PMMA layer on a gold surface, spin-coated using the same parameters as in the previous experiments. We find that the presence and spectral position of the PMMA vibrational bands are in good agreement between our angle-multiplexed approach and the IRRAS measurement. Moreover, our metasurface delivers a more than 50 times higher absorption signal due to the strongly enhanced near-field vibrational coupling.

Spectrometer-less sensor operation

The wide applicability of traditional angle-scanning SPR approaches originates from their high sensitivity and capability for spectrometer-less operation. To show that our metasurface-based concept can be implemented with similar device-level simplicity, we examine the spectral distribution of reflected light intensity in our measurements before and after PMMA deposition in more detail (Fig. 4A). We find that due to the low resonance background signal, the majority of the analyte-induced optical modulation occurs as reflectance changes close to the resonance peak itself (Fig. 4B).

Therefore, when illuminating the sensor metasurface with a broadband light source, the total reflectance signal for any given incidence angle is strongly correlated with the strength of the molecular absorption band at the corresponding resonance frequency. By recording the total reflectance intensity for all incidence angle steps, the full absorption signature of the molecular analyte can be retrieved over the spectral operating range of the metasurface. This detection method can be implemented using a broadband detector and light source, enabling

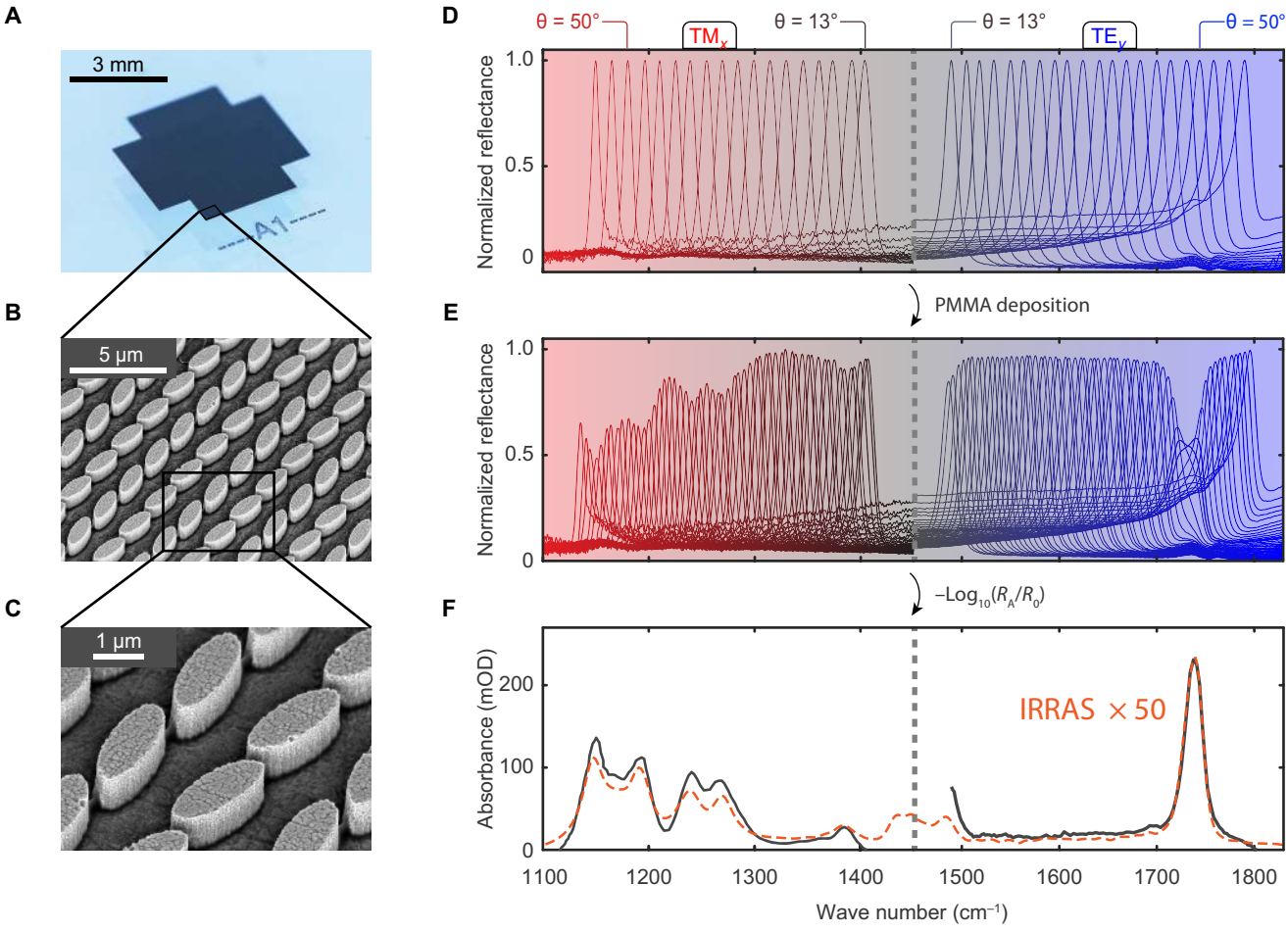

Fig. 3. Angle-multiplexed molecular fingerprint detection. (**A**) Photograph of a fabricated large-area all-dielectric metasurface used for reflection experiments. (**B** and **C**) Scanning electron microscopy micrographs of the metasurface confirm the homogeneity of the nanofabrication. (**D**) Normalized reflectance spectra of the metasurface before analyte coating. The angular range is from θ = 13° to θ = 60°, which corresponds to a wide spectral tuning range of 1120 to 1800 cm^{-1}. (**E**) Normalized reflectance spectra after deposition of a spin-coated PMMA thin film. Multiple molecular absorption bands of the PMMA are clearly visible as a distinct modulation of the reflectance spectra. (**F**) Absorbance spectrum in optical density (OD) units calculated from the reflectance envelopes before and after analyte coating. Agreement with independent IRRAS measurements is excellent, and a signal enhancement factor of around 50 is observed.

spectrometer-less operation. In this total reflectance configuration, the final spectral resolution of the approach is determined by both the resonance step size introduced above and the *Q*-factor of the resonances. In our experiments, we chose a resonance step size of around 1.5 cm^{-1} together with *Q*-factors of around 200, which yields an effective spectral resolution below 5 cm^{-1}. This resolution value is up to one order of magnitude narrower than the spectral feature size of the target samples' vibrational bands, such as those from proteins. Commonly used FTIR spectroscopy typically operates at a resolution of 8 to 4 cm^{-1} for protein studies. By moderately increasing the angular resolution and the resonance *Q*-factor (*18*), highly competitive spectral resolutions below 2 cm^{-1} could be achieved (fig. S4).

To demonstrate the viability of this approach, we evaluated the total reflectance intensities I_0 and I_A before and after PMMA deposition using spectral integration (Fig. 4B and fig. S5). The angle-dependent sensor signal of our AFR method was then calculated via $S_{AFR} = -\log_{10}(I_A/I_0)$. Since there is a one-to-one correspondence between the incidence angle and the metasurface resonance frequency (see Fig. 3D), the AFR signal is represented as a function of wave number.

The AFR signal for the PMMA layer clearly captures the multiple characteristic absorption features of the deposited polymer molecules (Fig. 4C). Efficient fingerprint retrieval is maintained even for spectrometer-less operation, and the AFR signal provides results similar to the previous spectroscopic evaluation of the peak reflectance attenuation (Fig. 3F). The disagreement in the spectral region around 1600 cm^{-1} arises because of a slight red shift of the resonance after analyte coating and the uneven spectral intensity profile of the used light source. This discrepancy can be minimized by using a light source with more even spectral power distribution. Note that the resonance red shift and uneven illumination does not affect the response in spectroscopic operation as can be seen in Fig. 3F.

To highlight the capabilities of broad spectral coverage of our sensor to chemically detect a wide range of different analytes, we performed a bioassay for the detection of human ODAM by using single-stranded DNA aptamers, which can specifically bind to ODAM (*28*). Since ODAM plays a key role in odontogenesis, it has been considered as a strong biomarker protein for diagnosing periodontal diseases (*29*, *30*). On the basis of a high correlation between the level of ODAM in gingival crevicular

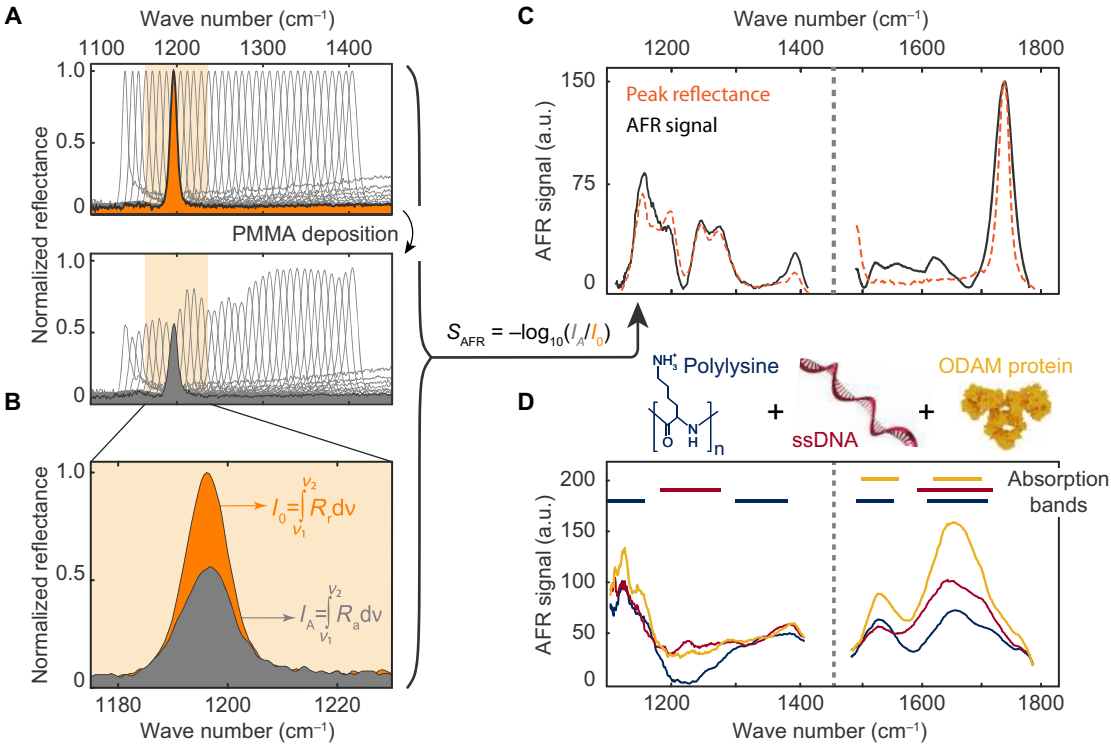

Fig. 4. Spectrometer-less angle-scanning molecular fingerprint detection and application to a multistep bioassay. (**A** and **B**) The high resonance sharpness and low reflectance background of our metasurface design over a broad tuning range enable the retrieval of vibrational fingerprint information from the total reflectance signals I_0 and I_A. (**C**) The AFR signal clearly reproduces the PMMA absorption fingerprint over 600 cm^{-1}, confirming the spectrometer-less detection capability of our approach. (**D**) The broad spectral coverage of the angle-multiplexed method enables chemically specific fingerprint detection of a wide range of analytes in a bioassay involving interactions of polylysine, DNA, and ODAM protein molecules. Multiple distinct absorption bands of these biomolecules are well resolved. ssDNA, single-stranded DNA.

fluid and the severity of periodontal diseases, the facile and fast detection of ODAM is expected to give an adequate treatment to patients in a timely manner and enable the early diagnosis of periodontal disorders. In addition, most of the current detection methods still need expert skills and laborious procedures to render a clinical diagnosis. Therefore, applying a bioassay based on ODAM-specific binding aptamers on our device could address the needs for an early, simple, and rapid diagnosis of periodontal diseases and their progression.

During the course of the bioassay, we first physisorbed polylysine molecules onto to the sensor surface, which produced strong absorption signal increases at multiple spectral positions of 1150, 1530, and 1640 cm^{-1}, which are connected to the backbone, amide II, and amide I absorption bands of the molecules, respectively (Fig. 4D). After polylysine deposition and rinsing with deionized water, single-stranded DNA molecules were incubated on the metasurface. Because of the negative net charge of DNA and the positively charged polylysine, the DNA aptamers bind to the surface through electrostatic interaction. The bound aptamer molecules produce distinct absorption signal increases at 1235 and 1650 cm^{-1}, which are well correlated with literature data of single-stranded DNA absorbance (*31*). The final step of the bioassay was the binding of ODAM protein to the single-stranded DNA aptamers, which could be detected by the strong signal increases at the characteristic amide I and amide II absorption bands at 1540 and 1660 cm^{-1} (Fig. 4D). The high signal-to-noise ratio of our angle-multiplexed detection approach allows us to resolve submonolayer analyte molecule amounts with a limit of detection of 3000 molecules/μm^2, which would correspond to a surface mass sensitivity of 0.27 pg/mm^2 (fig. S6). This level of sensitivity can be achieved in the spectrometer-less operation mode of our angle-scanning method, highlighting the potential of AFR-based sensors for realizing compact absorption fingerprint detectors.

DISCUSSION

We have demonstrated a novel metasurface-based mid-IR sensor approach, which simultaneously provides strong enhancement of the electromagnetic near fields and external tuning of the resonance frequency by controlling the incidence angle of light. By using straightforward angle-scanning reflectance measurements, we have obtained a multitude of ultrasharp ($Q > 100$) and highly surface-sensitive resonances over a wide spectral range from 1100 to 1800 cm^{-1} with a spectral tunability step size smaller than 1.5 cm^{-1}. We used this all-dielectric sensor metasurface to detect the characteristic mid-IR absorption fingerprints of surface-adsorbed molecules by correlating the reflectance signal at each incidence angle with the strength of the molecular absorption at the corresponding resonance frequency. We have shown that our method can be implemented using a broadband incoherent light source and a detector to enable the spectrometer-less retrieval of spectrally resolved molecular fingerprints. In comparison to other angle-scanning techniques such as SPR, our method provides not only high sensitivity but also chemical specificity, unlocking new opportunities in label-free biosensing. We have leveraged our AFR technique to detect the absorption signatures of polylysine, DNA aptamer, and ODAM protein molecules relevant for periodontal disease detection in a multistep bioassay over a broad spectral range, allowing detection of their association with

a highly competitive surface mass sensitivity of 0.27 pg/mm^2. Because our approach is capable of extracting absorption fingerprints without the need for bulky spectrometers or tunable lasers, it holds the potential for enabling a new toolkit of sensitive, cost-effective, and field-deployable sensors for a wide range of applications.

MATERIALS AND METHODS

Numerical calculations

The numerical simulations of the metasurface optical response for different illumination angles were performed using the frequency-domain finite-element method Maxwell solver from CST STUDIO SUITE 2017. The unit cell geometry was defined by the periodicities P_x = 4050 nm and P_y = 2340 nm, the long and short ellipse axes of A = 2250 nm and B = 900 nm, and the ellipse height of H = 800 nm. The ellipse orientation angle along the y axis was set to α = 10°. The resonator geometric parameters were chosen for optimal tradeoff between spectral tunability range, resonance quality factor, and the resonance background reflectance. The resonance tunability is set by the spectral separation between the main resonance and the first grating order, while the resonance background and quality factor is highly dependent on the ellipse eccentricity and ellipse tilt angle α.

The light incidence angle θ was varied from 0° to 60° for both TM_x (φ = 0°) and TE_y (φ = 90°) modes with 0.5° steps. The refractive index values for the germanium resonators and CaF_2 substrate were taken as n = 4.01 and n = 1.38 in the spectral range of 1000 to 1800 cm^{-1}. The germanium and CaF_2 materials are assumed to have no intrinsic losses in the corresponding spectral range.

Metasurface fabrication

Fabrication was performed on calcium fluoride (CaF_2) substrates, which have low absorption losses and a low refractive index in the mid-IR spectral range. A magnesium oxide (MgO) layer of 5-nm thickness was sputtered as a buffer layer for increased germanium layer stability on CaF_2 substrates. On top of the MgO layer, an 800-nm-thick germanium layer was deposited by direct current (DC) magnetron sputtering. The resonator pattern was defined using electron beam lithography in spin-coated double-layer PMMA (PMMA 495 K and PMMA 950 K) films. An Al_2O_3 hard mask of 20-nm thickness was deposited via electron beam evaporation and wet chemical lift-off process. The resonator pattern was subsequently transferred into the underlying germanium layer by fluorine-based dry plasma etching. To passivate the germanium surface, the resonators where uniformly coated with 10 nm Al_2O_3 by atomic layer deposition.

Analyte preparation

The PMMA resist analyte solution was produced by dissolving PMMA with an average weight of 350,000 g/mol in anisole with a concentration of 3 mg/ml. The thin film was deposited by spin-coating the PMMA solution (3 mg/ml) onto the metasurface using 6000-rpm spin speed. The same procedure was carried out for the IRRAS PMMA reference measurement.

For the bioassay measurements, polylysine was diluted in phosphate-buffered saline solution to a concentration of 100 µg/ml. The metasurface chip was incubated with the polylysine to allow polymer physisorption.

The single-stranded DNA aptamer molecules were prepared in 10 mM (pH 7.4) phosphate-buffered saline with 20 µM concentration and bound to the polylysine-coated chip surface. As an aptamer-specific binding molecule, human ODAM sample solution (0.25 mg/ml) was prepared by using the same buffer conditions as for DNA aptamer solution preparation. The used DNA sequence for the ODAM specific aptamer was as follows (*28*): 5′-CCATTCGTACGCAACAGGGATG-CATCGACTGTAAAC ACGTGGATGGCTCTGAATGC-3′.

Optical measurements

Optical performance of metasurfaces was characterized with a FTIR spectrometer (Bruker Vertex 70v) equipped with a variable angle reflection accessory (Bruker A519/Q). The reference measurement for the spin-coated thin PMMA layer was carried out using IRRAS. At first, a reference reflectance spectrum of gold mirror was measured, after which the reflectance from the spin-coated PMMA thin film was measured. The spectrum of the analyte was measured with a FTIR spectrometer (Bruker Vertex 80v) using a variable angle reflection accessory (Harrick SEAGULL). The measurements were made at 80° light incidence angle with transverse magnetic polarized light.

SUPPLEMENTARY MATERIALS

Supplementary material for this article is available at http://advances.sciencemag.org/cgi/content/full/5/5/eaaw2871/DC1

Supplementary Text

Fig. S1. The lattice distribution of the impedance element $Z_S^{(m,n)}$ and $Z_M^{(m,n)}$.

Fig. S2. The change of the effective inductance and elastance under different incident angles.

Fig. S3. Experimental data of resonance position and quality factor.

Fig. S4. Spectral resolution as a function of Q-factor for different values of the resonance step size.

Fig. S5. Resonance background calculation and AFR signal correction.

Fig. S6. Noise and limit of detection.

References (*32*–*34*)

REFERENCES AND NOTES

1. M. E. Germain, M. J. Knapp, Optical explosives detection: From color changes to fluorescence turn-on. *Chem. Soc. Rev.* **38**, 2543–2555 (2009).
2. F. Long, A. Zhu, H. Shi, Recent advances in optical biosensors for environmental monitoring and early warning. *Sensors* **13**, 13928–13948 (2013).
3. X. Fan, I. M. White, S. I. Shopova, H. Zhu, J. D. Suter, Y. Sun, Sensitive optical biosensors for unlabeled targets: A review. *Anal. Chim. Acta* **620**, 8–26 (2008).
4. F. B. Myers, L. P. Lee, Innovations in optical microfluidic technologies for point-of-care diagnostics. *Lab Chip* **8**, 2015–2031 (2008).
5. A. M. Armani, R. P. Kulkarni, S. E. Fraser, R. C. Flagan, K. J. Vahala, Label-free, single-molecule detection with optical microcavities. *Science* **317**, 783–787 (2007).
6. C. Ciminelli, C. M. Campanella, F. Dell'Olio, C. E. Campanella, M. N. Armenise, Label-free optical resonant sensors for biochemical applications. *Prog. Quantum Electron.* **37**, 51–107 (2013).
7. P. Singh, SPR Biosensors: Historical perspectives and current challenges. *Sens. Actuators B* **229**, 110–130 (2016).
8. J. Homola, Surface plasmon resonance sensors for detection of chemical and biological species. *Chem. Rev.* **108**, 462–493 (2008).
9. B. Stuart, *Infrared Spectroscopy*, in Kirk-Othmer Encyclopedia of Chemical Technology (John Wiley & Sons Inc., 2015), pp. 1–18.
10. A. Barth, Infrared spectroscopy of proteins. *Biochim. Biophys. Acta* **1767**, 1073–1101 (2007).
11. R. Adato, A. A. Yanik, J. J. Amsden, D. L. Kaplan, F. G. Omenetto, M. K. Hong, S. Erramilli, H. Altug, Ultra-sensitive vibrational spectroscopy of protein monolayers with plasmonic nanoantenna arrays. *Proc. Natl. Acad. Sci. U.S.A.* **106**, 19227–19232 (2009).
12. O. Limaj, D. Etezadi, N. J. Wittenberg, D. Rodrigo, D. Yoo, S. H. Oh, H. Altug, Infrared plasmonic biosensor for real-time and label-free monitoring of lipid membranes. *Nano Lett.* **16**, 1502–1508 (2016).
13. C. Huck, F. Neubrech, J. Vogt, A. Toma, D. Gerbert, J. Katzmann, T. Härtling, A. Pucci, Surface-enhanced infrared spectroscopy using nanometer-sized gaps. *ACS Nano* **8**, 4908–4914 (2014).
14. L. Dong, X. Yang, C. Zhang, B. Cerjan, L. Zhou, M. L. Tseng, Y. Zhang, A. Alabastri, P. Nordlander, N. J. Halas, Nanogapped Au antennas for ultrasensitive surface-enhanced infrared absorption spectroscopy. *Nano Lett.* **17**, 5768–5774 (2017).
15. F. Neubrech, C. Huck, K. Weber, A. Pucci, H. Giessen, Surface-enhanced infrared spectroscopy using resonant nanoantennas. *Chem. Rev.* **117**, 5110–5145 (2017).

16. X. Gai, D.-Y. Choi, B. Luther-Davies, Negligible nonlinear absorption in hydrogenated amorphous silicon at 1.55 μm for ultra-fast nonlinear signal processing. *Opt. Express* **22**, 9948–9958 (2014).
17. A. Arbabi, Y. Horie, M. Bagheri, A. Faraon, Dielectric metasurfaces for complete control of phase and polarization with subwavelength spatial resolution and high transmission. *Nat. Nanotechnol.* **10**, 937–943 (2015).
18. S. Campione, S. Liu, L. I. Basilio, L. K. Warne, W. L. Langston, T. S. Luk, J. R. Wendt, J. L. Reno, G. A. Keeler, I. Brener, M. B. Sinclair, Broken symmetry dielectric resonators for high quality factor fano metasurfaces. *ACS Photonics* **3**, 2362–2367 (2016).
19. Q. Wang, E. T. F. Rogers, B. Gholipour, C.-M. Wang, G. Yuan, J. Teng, N. I. Zheludev, Optically reconfigurable metasurfaces and photonic devices based on phase change materials. *Nat. Photonics* **10**, 60–65 (2016).
20. A. Tittl, A. Leitis, M. Liu, F. Yesilkoy, D.-Y. Choi, D. N. Neshev, Y. S. Kivshar, H. Altug, Imaging-based molecular barcoding with pixelated dielectric metasurfaces. *Science* **360**, 1105–1109 (2018).
21. S. Kruk, Y. Kivshar, Functional meta-optics and nanophotonics governed by Mie resonances. *ACS Photonics* **4**, 2638–2649 (2017).
22. S. M. Kamali, E. Arbabi, A. Arbabi, Y. Horie, M. S. Faraji-Dana, A. Faraon, Angle-multiplexed metasurfaces: Encoding independent wavefronts in a single metasurface under different illumination angles. *Phys. Rev. X* **7**, 041056 (2017).
23. K. Koshelev, S. Lepeshov, M. Liu, A. Bogdanov, Y. Kivshar, Asymmetric metasurfaces with high-*Q* resonances governed by bound states in the continuum. *Phys. Rev. Lett.* **121**, 193903 (2018).
24. M. V. Rybin, K. L. Koshelev, Z. F. Sadrieva, K. B. Samusev, A. A. Bogdanov, M. F. Limonov, Y. Kivshar, High-*Q* supercavity modes in subwavelength dielectric resonators. *Phys. Rev. Lett.* **119**, 243901 (2017).
25. C. W. Hsu, B. Zhen, A. D. Stone, J. D. Joannopoulos, M. Soljačić, Bound states in the continuum. *Nat. Rev. Mater.* **1**, 16048 (2016).
26. D. C. Marinica, A. G. Borisov, S. V. Shabanov, Bound states in the continuum in photonics. *Phys. Rev. Lett.* **100**, 183902 (2008).
27. M. Liu, D. A. Powell, R. Guo, I. V. Shadrivov, Y. S. Kivshar, Polarization-induced chirality in metamaterials via optomechanical interaction. *Adv. Opt. Mater.* **5**, 1–8 (2017).
28. B. H. Lee, S. H. Kim, Y. Ko, J. C. Park, S. Ji, M. B. Gu, The sensitive detection of ODAM by using sandwich-type biosensors with a cognate pair of aptamers for the early diagnosis of periodontal disease. *Biosens. Bioelectron.* **126**, 122–128 (2019).
29. H. K. Lee, S. Ji, S. J. Park, H. W. Choung, Y. Choi, H. J. Lee, S. Y. Park, J. C. Park, Odontogenic ameloblast-associated protein (ODAM) mediates junctional epithelium attachment to teeth via integrin-odam-rho guanine nucleotide exchange factor 5 (ARHGEF5)-RhoA signaling. *J. Biol. Chem.* **290**, 14740–14753 (2015).
30. H. K. Lee, S. J. Kim, Y. H. Kim, Y. Ko, S. Ji, J. C. Park, Odontogenic ameloblast-associated protein (ODAM) in gingival crevicular fluid for site-specific diagnostic value of periodontitis: A pilot study. *BMC Oral Health* **18**, 148 (2018).
31. B. R. Wood, The importance of hydration and DNA conformation in interpreting infrared spectra of cells and tissues. *Chem. Soc. Rev.* **45**, 1980–1998 (2016).
32. M. Liu, D. A. Powell, I. V. Shadrivov, M. Lapine, Y. S. Kivshar, Spontaneous chiral symmetry breaking in metamaterials. *Nat. Commun.* **5**, 4441 (2014).
33. R. Adato, A. Artar, S. Erramilli, H. Altug, Engineered absorption enhancement and induced transparency in coupled molecular and plasmonic resonator systems. *Nano Lett.* **13**, 2584–2591 (2013).
34. H. P. Erickson, Size and shape of protein molecules at the nanometer level determined by sedimentation, gel filtration, and electron microscopy. *Biol. Proced. Online* **11**, 32–51 (2009).

Acknowledgments: We would like to thank D. Neshev and F. Yesilkoy for fruitful discussions. **Funding:** The research leading to these results has received funding from the European Research Council (ERC) under grant agreement no. 682167 VIBRANT-BIO and the European Union Horizon 2020 Framework Programme for Research and Innovation under grant agreement no. 665667 (call 2015) and no. 777714 (NOCTURNO project). We also acknowledge École Polytechnique Fédérale de Lausanne and Center of MicroNano Technology for nanofabrication. **Author contributions:** A.L., A.T., Y.S.K., and H.A. conceived and designed the research; A.L. fabricated the dielectric metasurfaces; A.L. and A.T. carried out optical measurements and analyzed the data; A.L. and M.L. carried out numerical simulations; A.L. and B.H.L. prepared the analyte solutions; M.B.G. provided the biomolecules used in the study; and all authors contributed to writing the manuscript. **Competing interests:** The authors declare that they have no competing interests. **Data and materials availability:** All data needed to evaluate the conclusions in the paper are present in the paper and/or the Supplementary Materials. Additional data related to this paper may be requested from the authors.

Submitted 6 December 2018
Accepted 2 April 2019
Published 17 May 2019
10.1126/sciadv.aaw2871

Citation: A. Leitis, A. Tittl, M. Liu, B. H. Lee, M. B. Gu, Y. S. Kivshar, H. Altug, Angle-multiplexed all-dielectric metasurfaces for broadband molecular fingerprint retrieval. *Sci. Adv.* **5**, eaaw2871 (2019).

Angle-multiplexed all-dielectric metasurfaces for broadband molecular fingerprint retrieval

Aleksandrs Leitis, Andreas Tittl, Mingkai Liu, Bang Hyun Lee, Man Bock Gu, Yuri S. Kivshar and Hatice Altug

Sci Adv **5** (5), eaaw2871.
DOI: 10.1126/sciadv.aaw2871